JOURNAL OF SYNCHROTRON RADIATION
ISSN 1600-5775

Time- and spatial-resolved XAFS spectroscopy in a single shot: new analytical possibilities for *in situ* material characterization

Ana Guilherme Buzanich,* Martin Radtke, Uwe Reinholz, Heinrich Riesemeier and Franziska Emmerling

Federal Institute for Materials Research and Testing (BAM), Division 1.3 Structure Analysis, Richard-Willstaetter-Strasse 11, 12489 Berlin, Germany. *Correspondence e-mail: ana.buzanich@bam.de

Received 18 December 2015
Accepted 8 March 2016

Edited by R. W. Strange, University of Liverpool, UK

Keywords: single-shot XAFS; time resolution; spatial resolution; divergent XAFS.

A new concept that comprises both time- and lateral-resolved X-ray absorption fine-structure information simultaneously in a single shot is presented. This uncomplicated set-up was tested at the BAMline at BESSY-II (Berlin, Germany). The primary broadband beam was generated by a double multilayer monochromator. The transmitted beam through the sample is diffracted by a convexly bent Si (111) crystal, producing a divergent beam. This, in turn, is collected by either an energy-sensitive area detector, the so-called color X-ray camera, or by an area-sensitive detector based on a CCD camera, in θ–2θ geometry. The first tests were performed with thin metal foils and some iron oxide mixtures. A time resolution of lower than 1 s together with a spatial resolution in one dimension of at least 50 µm is achieved.

1. Introduction

X-ray-based techniques are an excellent analytical choice for material characterization, as they provide fast elemental, compositional and structural information, non-destructively. Among these techniques, X-ray absorption spectroscopy (XAS) in its numerous configurations is an excellent method for chemical speciation and structural properties of matter (both crystalline and amorphous). In the field of XAS, X-ray absorption fine-structure (XAFS) spectroscopy is commonly used. This technique entails both XANES (X-ray absorption near-edge structure) and EXAFS (extended X-ray absorption fine-structure) spectroscopy, providing information about the chemical state and near-range coordination geometry, respectively (Bunker, 2010; Newville, 2004).

The possibility of performing such measurements on chemically heterogeneous samples, which change over time and space, is of great importance. These *in situ* and *operando* analyses are often carried out by means of XAFS and require time and spatial resolution. Bordiga *et al.* (2013) present an excellent review on *in situ* XAS to study the reactivity of surface species in heterogeneous catalysts. A consistent scientific background as well as the applicability of various configurations of XAS is thoroughly discussed. Examples of *in situ* studies by means of XANES/EXAFS can be found in the literature (Bare *et al.*, 2010; Koziej *et al.*, 2009; Kleymenov *et al.*, 2012; Gawelda, 2006), which require monochromatic radiation with energy scans. These measurements have to be performed at high-flux sources, normally found at large-scale facilities such as electron storage rings.

In the last few years several attempts have been made to improve the time resolution of XAFS measurements such as

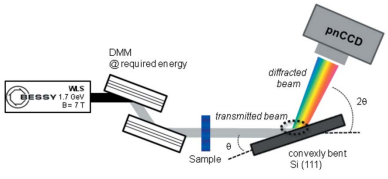

the replacement of the time-consuming stepwise variation of the monochromator by other methods: Quick-EXAFS (QEXAFS) is well established (Frahm *et al.*, 2009). In the most recent QEXAFS set-ups the polychromatic beam at a synchrotron radiation source is monochromated by a continuously oscillating channel-cut crystal before the beam passes the sample (Stötzel *et al.*, 2011). The recently developed QEXAFS monochromators enable scan rates of up to about 20–80 spectra per second, each one covering a 1 keV energy range.

Other experimental set-ups for time-resolved XANES measurements, so-called dispersive-XAFS, have also been reported and are well established at synchrotrons such as the European Synchrotron Radiation Facility (ESRF), Soleil, Diamond Light Source and SPring-8 (Flank *et al.*, 1983; D'Acapito *et al.*, 1992; Hagelstein *et al.*, 1989; Bhattacharyya *et al.*, 2009). The classical dispersive-XAFS mode is well established and uses position-sensitive detectors or CCD cameras. An example is one at the ID24 beamline at the ESRF. Instead of exposing the CCD camera directly to the X-ray beam, a scintillating screen is coupled to the active part of the CCD by a lens system. By changing the scintillating screen, energy and time resolution can be easily adapted to the experimental needs. The 'white' or 'pink' beam is focused by a bent polychromator into a few micrometers in width (where the sample can be located). Behind the focus the beam diverges again, allowing the simultaneous collection of the whole transmitted spectrum in a single shot (Pascarelli *et al.*, 1999; Labiche *et al.*, 2007). A more sophisticated version of dispersive-XAFS at the ESRF consists of gathering the necessary horizontal divergency obtained from the source (bending magnet). This is achieved by using several optical elements until the radiation interacts with the sample, making this optical scheme more suited for microfocus/high-brilliance applications (Pascarelli *et al.*, 2006).

In this manuscript, we present a newly developed set-up that combines both time- and simultaneous spatial-resolution, while acquiring an XAFS spectrum in a single shot. This uncomplicated set-up uses as dispersive element a Si (111) crystal, which is placed after the sample and is convexly bent to produce a divergent beam onto the two-dimensional detector. The most attractive features are: (i) this set-up is static, not even requiring sample displacement for the spatial resolution; (ii) since there is no focusing beam needed, a simple and cheap Si (111) wafer as crystal analyzer can be used. As explained in detail below, a time resolution of below 1 s and a spatial resolution in one dimension of at least 50 µm are expected. First tests on iron oxides prove the feasibility of our approach.

2. Experimental set-up

In Fig. 1 a sketch of the newly developed set-up for single-shot XANES (*a*) and single-shot EXAFS (*c*) is presented with details of the respective detectors used [(*b*) and (*d*)]. In both cases the incident beam interacts with the sample and the

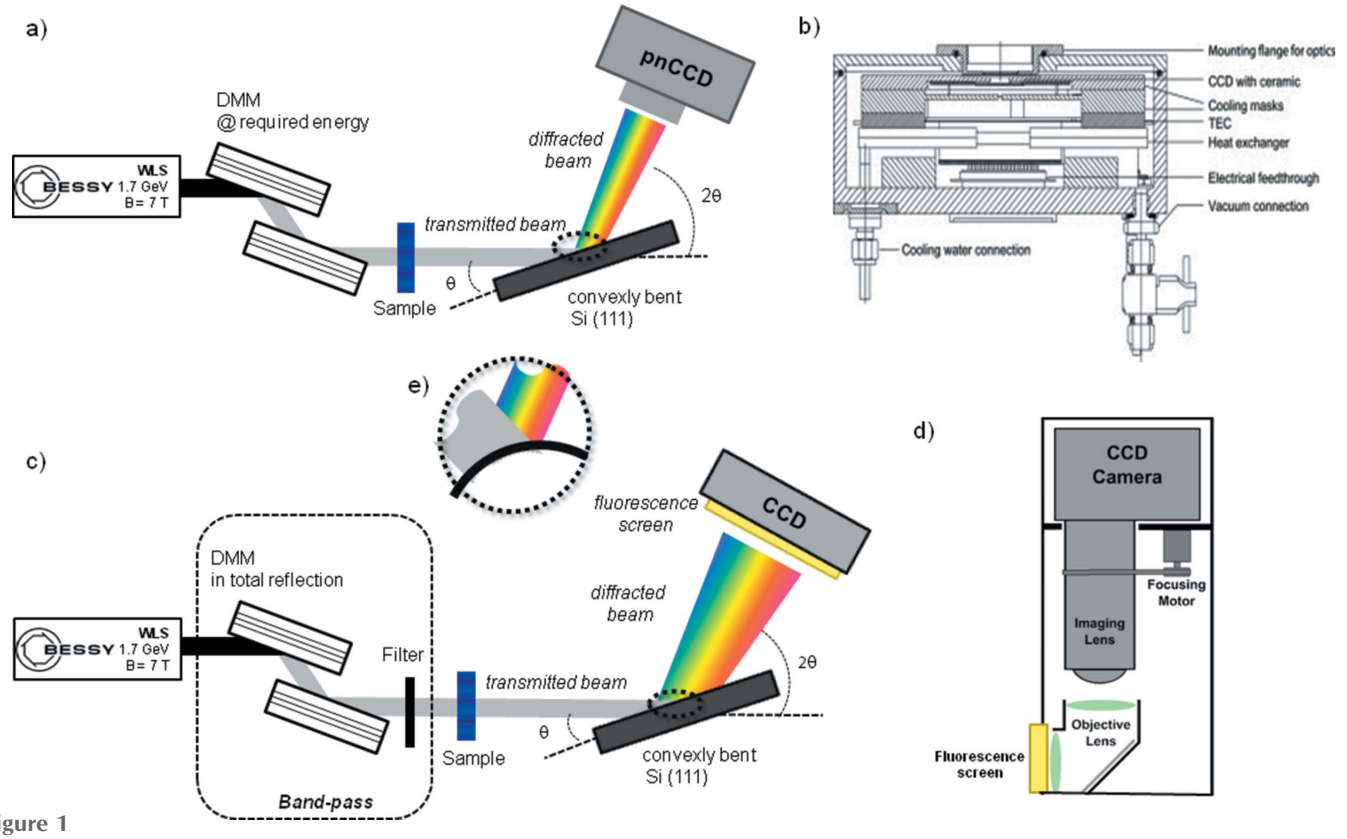

Figure 1
(*a*) Sketch of the set-up used for single-shot XANES. (*b*) Details of the detector (pnCCD chip; Ordavo *et al.*, 2011). (*c*) Sketch of the set-up used for single-shot EXAFS. (*d*) Details of the X-ray area-sensitive detector based on a CCD (Williams *et al.*, 2012). (*e*) Detail of the convex shape of the crystal.

transmitted part is diffracted by a convexly bent Si (111) crystal. For the single-shot XANES approach, the divergent beam was detected by an energy-sensitive area detector, the pnCCD chip of the color X-ray camera (CXC). For the single-shot EXAFS, an area-sensitive detector based on a CCD camera was used. The bent Si (111) crystal and the detector were placed under conventional θ–2θ diffraction geometry.

Detailed information about the chosen elements for these experiments is provided in the following.

2.1. Single-shot XANES

The beam was filtered by a double multilayer monochromator (DMM). The two multilayer (ML) mirrors consist of single-crystalline Si substrates with a usable area of 300 mm $\times$ 60 mm covered with W/Si coatings. On each mirror, 300 single layers with a $2d$ spacing of 5.8 nm (1.2/1.7 nm, W/Si) are deposited. Furthermore, from the rocking curve previously measured elsewhere (Riesemeier *et al.*, 2005) a bandwidth $\Delta E/E$ of about 1.7% [full width at half-maximum (FWHM)] was obtained. If we consider a central incident energy of 7 keV (covering the Fe XANES range), a usable range of about 180 eV (1.5 $\times$ FWHM) is obtained.

A bent Si (111) wafer (SIEGERT WAFER GmbH, Aachen, Germany), with a thickness of 0.53 mm and 100 mm diameter, was used as a dispersive element. In order to control the bending radius a device was designed and manufactured in-house (Fig. 2). The wafer was placed onto a rod (blue element) and held at three points. The other two positions form the actual bending mechanism, where one side is fixed (dark-green element) and one side is adjustable in depth by means of a screw (pink element). By turning the screw the wafer is convexly bent. The number of turns (or the applied pressure) defines the bending radius of the crystal. The radius must be adjusted until one obtains a divergent beam that comprises the desired energies from the transmitted beam (Fig. 1).

The achievable experimental energy resolution is limited by its intrinsic resolution ($\Delta E/E \simeq 1.4 \times 10^{-4}$) together with the curvature radius. Stronger bending leads to a larger reflected energy range and a poorer energy resolution, however. The detectable energy range is restricted by the detector size. Hence, for higher or lower desired energies the curvature radius and the geometry has to be adjusted.

The calculation of the curvature radius has to be performed prior to the measurements. We take the lowest and the highest energy within the required range of analysis. Let us assume that we want to investigate the Fe K-edge (7112 eV) and for XANES we want a 200 eV range. We take 7100 eV as lowest energy and 7300 eV as highest. Afterwards, the Bragg equation was used for the calculation of the incident angles.

Although the X-rays diverge due to the convexly shaped crystal, the curvature radius (r) can be easily calculated by using the virtually convergent X-rays beam (Fig. 2c). The intersection point corresponds to the center of the circumference and its distance to the surface of the crystal is the radius. Taking the geometric relationship drawn in Fig. 2(c) (blue and red dashed lines), we obtain the radius, r, given as

$$r = \frac{\mathrm{BW}}{(\sin\beta - \sin\alpha)}, \tag{1}$$

where BW is the beam width (which we consider now to be 10 mm) and α and β are the adjacent angles to the incoming angles θ_1 and θ_2, respectively. In our example a value of r = 4589 mm is obtained.

The CXC was developed and tested by the Institute for Scientific Instruments GmbH (IfG, Berlin, Germany), the Federal Institute for Materials Research and Testing (BAM), PNSensor GmbH (Munich, Germany) and the Institute for Applied Photonics eV (IAP, Berlin, Germany). The CXC

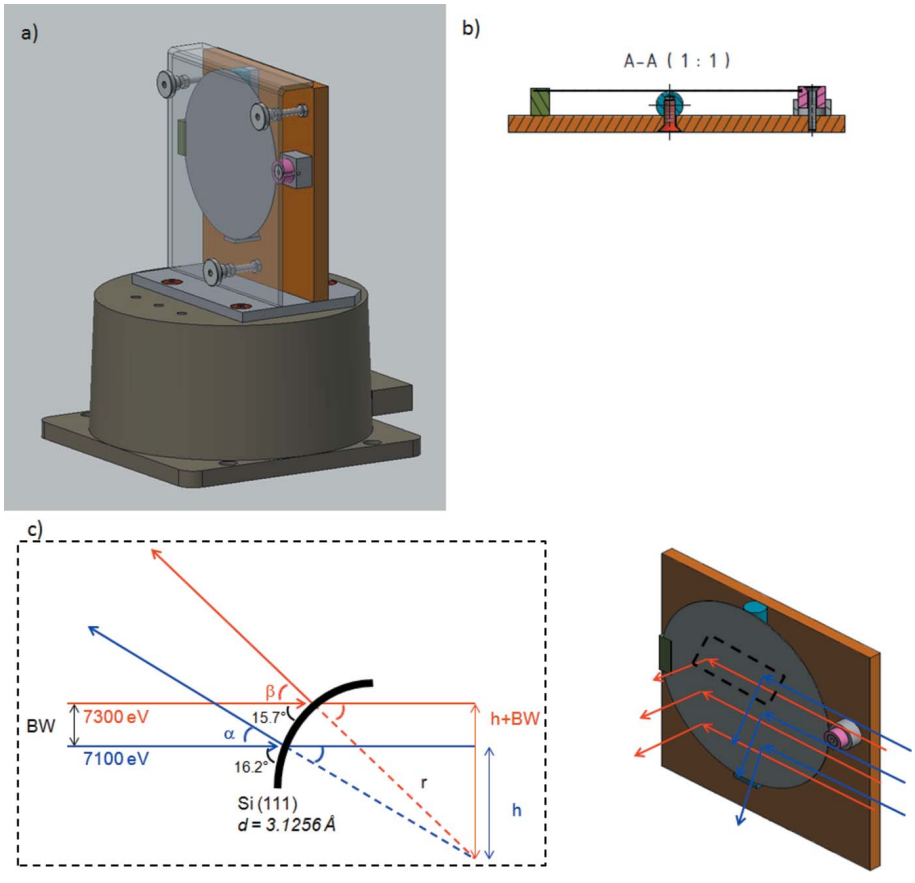

Figure 2
'Wafer bender'. (a) Overall sketch of the device in which the wafer is placed and bent. (b, c) Details of the working principle for the calculation of the curvature radius, required for the desired energy range.

consists of a pnCCD chip with 264 × 264 pixels (developed by PNSensor). If used in single-counting mode, for every photon the energy and the location on the chip is determined. A spatial resolution of 48 µm over an imaging area of 12.7 mm × 12.7 mm is obtained. It is sensitive to photons in the energy region between 3 and 17 keV above 50%, limited by a 50 µm beryllium window, and a sensitive chip thickness of 450 µm. The readout rate of the actual chip is 1000 Hz (Scharf *et al.*, 2011).

As the CXC in spectroscopic mode has a processing limit of about two million photons, the initial flux density (about 10^{10} s^{-1} mm^{-2}) for Fe-*K* delivered by the DMM has to be diminished. Therefore, the flux density at the CXC after passing through all the devices of the experiment was previously calculated and optimized by using a 350 µm-thick aluminium filter to avoid overload of the CXC. In this case, and taking into account the absorption in the sample and reflectivity of the bent crystal, a total flux density of about 6×10^6 s^{-1} mm^{-2} was obtained.

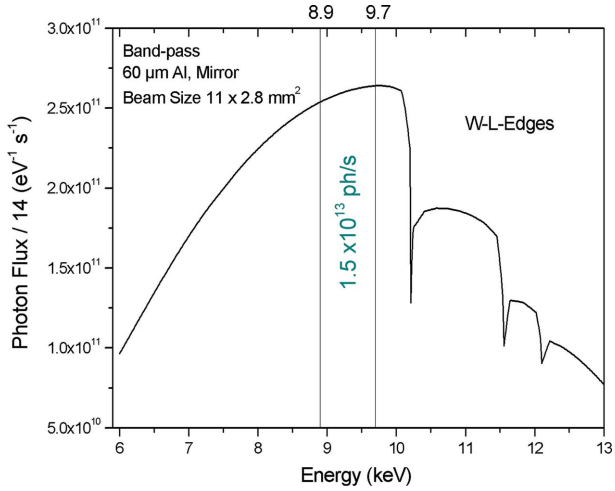

Figure 3
Graphical representation of the photon flux obtained by the 'band-pass' between DMM as mirror and a 60 µm-thick Al filter. For the EXAFS measurements of Cu-*K*, a total photon flux of 1.5×10^{13} photons s^{-1} is obtained.

2.2. Single-shot EXAFS

For this experiment, the detector and the source were adapted to the required energy bandwidth for the whole EXAFS spectrum. As the chip area of the pnCCD in the CXC is of 12.7 mm × 12.7 mm only, it is not possible to obtain the extended part of the absorption spectrum. For this purpose a fluorescence screen combined with an area-sensitive detector based on a CCD camera was used (Fig. 1*c*). The CCD camera is a EEV CCD42_40 model (Princeton Instruments, New Jersey, USA) from VersArray® Family of Camera, with 2048 × 2048 pixels. A spatial resolution of 13.5 µm per pixel allows an imaging area of 27.6 mm × 27.6 mm. It works under a Peltier cooling mechanism and has an automatic shutter trigger. The camera controller allows the read rate, on-chip binning parameters and regions of interest to be specified under the software control (WinView/32).

One other important feature of the CCD is the bit depth (n), which is 16 in our case. The camera records values between 0 and 2^n, for the contrast pattern. This pattern is a direct measure of the absorption profile from the sample. This profile is corrected to the flat-field and the resulting profile is our EXAFS spectrum. The imaging treatment was performed using *ImageJ* software (Schneider *et al.*, 2012). Another different aspect of this set-up is the application of a so-called 'band-pass' as source. The combination of the DMM in total reflection mode (also known as 'mirror' mode) together with a filter allows the optimal energy bandwidth required for the EXAFS to be chosen for the element of interest. For example, we can adjust the DMM to totally reflect all energies until 10 keV and combine it with a 60 µm-thick Al filter, for which the transmission increases greatly from 6 keV. In the end, this combination results in a 'band-pass' according to Fig. 3 [simulated with *RAY* software (Schäfers, 2008)]. For the EXAFS measurements of Cu-*K*, a total photon flux of 1.5×10^{13} photons s^{-1} is obtained. Since the DMM is composed of W (as mentioned above), the characteristic W *L*-edges are visible on this energy scale.

3. 'Proof of principle': results and discussion

3.1. Single-shot XANES

Time- and simultaneous spatial-resolved XANES measurements were tested on reference metal foils and on prepared Fe-compounds containing different oxidation states.

All measurements were acquired by the pnCCD in 'deposited energy' mode. This means the number of electrons (current) generated by the photon hits at each pixel is counted and accumulated during the time of measurement, much like using an ionization chamber. The accumulated current is proportional to the absorption in the sample, *i.e.* the higher the current the lower the absorption.

Furthermore, a measurement without sample ('empty') was taken. This provides a measure of the system's 'dark current', allowing compensation for possible inhomogeneities inherent to the setup [*e.g.* from the Si (111) crystal]. Afterwards the real measurement corresponds to the measurement of the sample corrected to the dark field, which will be our XANES data.

All data here-on presented were read by an in-house-developed routine in IDL® 8.3 that loads the raw data stored from the CXC (*.h5 files), reads out the deposited energy, corrects it to the dark field and saves them in ASCII format. Afterwards the XANES data were treated and normalized using *Athena* software (Ravel & Newville, 2005).

For the energy calibration, a Si (111) double-crystal monochromator (DCM) was chosen as first element instead of the DMM to provide a monochromatic excitation beam. An energy range of 300 eV was scanned in 10 eV steps. The channel at which the maximum intensity appears in the CXC was determined. A linear relationship between channel and energy is obtained according to the equation

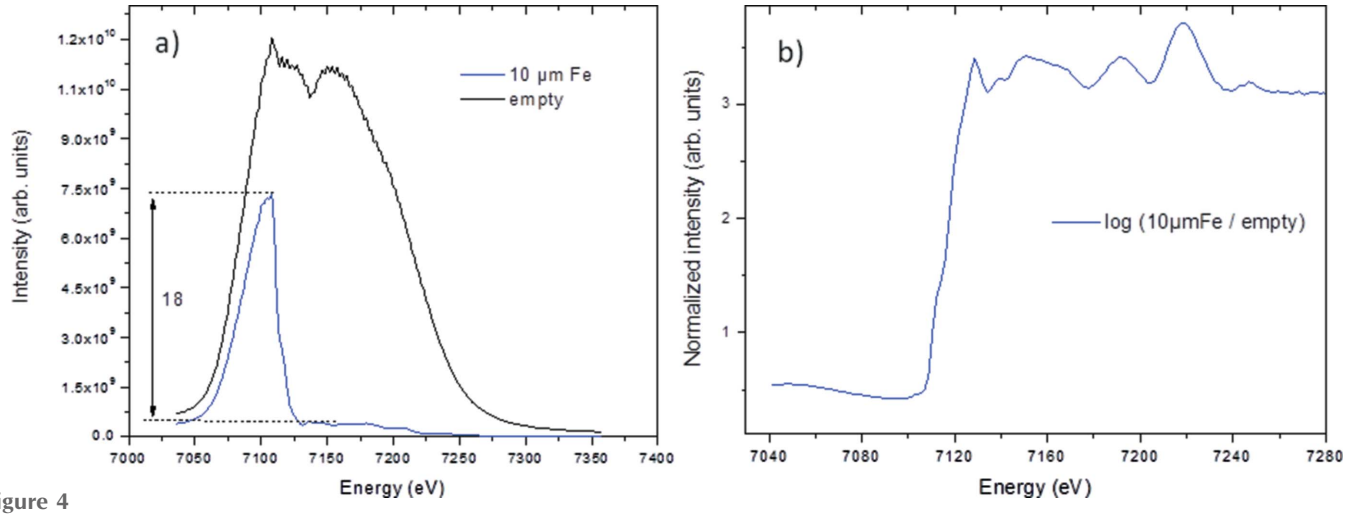

Figure 4
(*a*) Intensity profile obtained for a 10 µm-thick Fe-metal foil and for an 'empty' measurement. (*b*) XANES spectrum of the 10 µm Fe foil; intensity normalized to the dark field, measurement time 5 min.

$$y\ (\text{eV}) = 7417.2 - 1.82x\ (\text{pixel}). \qquad (2)$$

For this set-up, an average resolution of 1.8 eV per channel was obtained, within this energy range.

3.1.1. Measurements on metallic reference foils: time resolution. First measurements were performed on a 10 µm-thick Fe-metal foil, with a beam height of 8 mm and width of 10 mm. The DMM was set to the Fe *K*-edge energy (7112 eV) with a 200 eV bandwidth around the central energy. In Fig. 4(*a*) the intensity profile obtained for the 10 µm-thick Fe foil as well as the 'dark field' are shown. The biggest changes are noticeable after the Fe *K*-edge (at energy 7112 eV, channel 180), where an edge jump of about 18 was obtained. The XANES spectrum is obtained by normalizing the intensity profile of the foil to the dark field, which is plotted in Fig. 4(*b*). The measurement time was 5 min.

The 10 µm-thick Fe foil was used to check the signal-to-noise ratio at different acquisition times: 60 s, 30 s, 10 s, 5 s and 1 s. In Fig. 5 the measured XANES spectra together with the intensity map distribution obtained by the CXC are depicted. A conventionally measured XANES spectrum of the same reference foil is also presented. The absorption features obtained in a few seconds are quite similar to those in conventional XANES. Depending on the required statistics for the observed features, a time resolution down to 1 s is feasible.

3.1.2. Measurements on Fe_xO_x compounds: time- and lateral-resolution. As the CXC is an energy-sensitive area detector and offers the possibility of simultaneously providing time- and spatial-resolution in one dimension, this means that one can distinguish different oxidation states within the analyzed sample area. For this purpose two different Fe-oxide compounds were prepared, characterized by X-ray powder diffraction and placed in a sample holder. In Fig. 6 a scheme of this principle together with the sample information and obtained spectra are displayed.

γ-Fe_2O_3 and FeO in powder were prepared and placed in a 1 mm-thick sample holder to obtain an edge jump of about 10. For this purpose, both powders were diluted with boron nitride in order to fill the whole 1 mm-thick holder. In this case the different oxides were separated by 1 mm spacing (Fig. 6*a*). A beam of 8 mm height was used to cover both oxidation states. The transmitted signal, after being diffracted by the bent crystal, carries information about both oxidation states, recorded at once by the pnCCD (Fig. 6*b*). As mentioned above, the measurements were carried out in 'deposited energy mode', which results in the intensity map displayed in Fig. 6(*c*). The achievable lateral resolution in this geometry is limited by the pixel size of the pnCCD detector, which is 48 µm in our case. The acquired spectra were fitted and normalized using *Athena* software (Ravel & Newville, 2005). The two oxidation states could be distinguished in one shot (Fig. 6*d*), exhibiting the expected edge shift of about 5 eV (better visible by the first-derivative plot within the same figure).

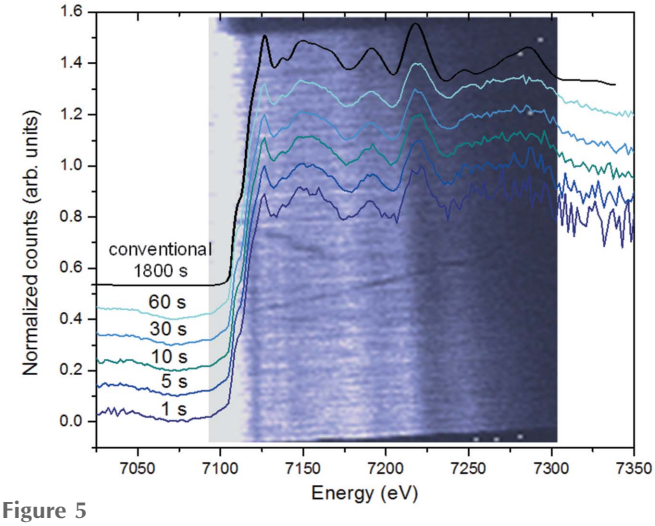

Figure 5
XANES profile for the different acquisition times (60 s, 30 s, 10 s, 5 s and 1 s) together with the intensity distribution map obtained by the CXC and conventional XANES spectrum.

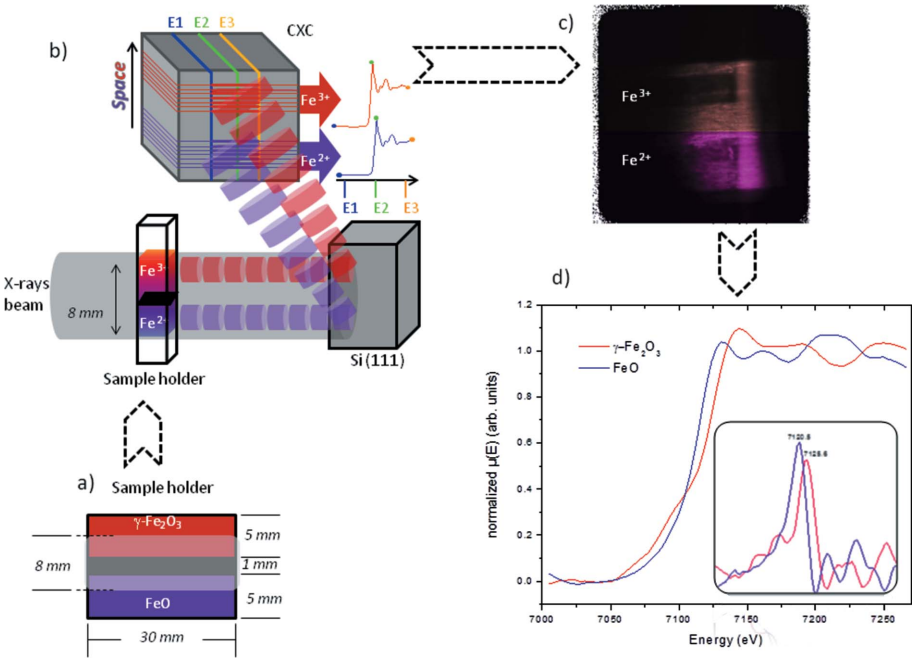

Figure 6
Principle for simultaneous time- and lateral-resolved XANES measurements: (*a*) Fe_2O_3 and FeO in sample holder; (*b*) sketch of the used setup; (*c*) intensity map obtained by the CXC; (*d*) correspondent spectra of the two Fe-oxides (γ-Fe_2O_3 and FeO); measurement time 10 min.

3.2. Single-shot EXAFS

The same procedure as explained in §3.1.2 was applied. The tests were performed on a Cu-metallic reference foil. As such, for the whole EXAFS range, the set-up was optimized for allowing an energy range of about 770 eV. Considering the intrinsic resolution of the Si (111) crystal, a binning of 2 of the CCD was chosen (1024 pixels), which results in an energy resolution about 50% better than the intrinsic one of the crystal.

For the energy calibration, a total energy range of 660 eV Cu-*K* was scanned. The pixel at which the maximum intensity appears in the CCD was determined. A linear relationship between pixel and energy was obtained, according to the equation

$$y\ (\text{eV}) = 8897.2 + 0.75x\ (\text{pixel}). \quad (3)$$

For this set-up, an average resolution of 0.75 eV pixel^{-1} was obtained, within this energy range.

3.2.1. Measurements on a Cu-metallic reference foil: time resolution. The first experimental tests were performed on a 12.5 µm-thick Cu-metallic foil, which results in an absorption jump of about 16. For this experiment a 2 × 4 binning of the CCD was chosen. With this configuration an area of 1024 × 62 pixels of the camera was illuminated, which actually corresponds to 27.6 mm × 3.3 mm [(1024 × 2 × 13.5) µm × (62 × 4 × 13.5) µm].

The measurement time was 6 s and a respective flat-field correction was applied. Fig. 7(*a*) shows the resulting intensity pattern from the 12.5 µm-thick Cu foil. Fig. 7(*b*) shows the profile obtained within the whole area. The stability of the set-up can be checked by analyzing the consistency of the flat-field. Fig. 7(*c*) shows the intensity pattern of the division of two measurements of the flat-field and the respective profile is plotted in Fig. 7(*d*). The flat-field is quite consistent, as the average of the profile is kept close to unity along the whole illuminated area.

When we look closely at the single EXAFS profiles from the whole 1024 × 62 pixels ROI (Fig. 7*c*), differences in the absorption features are noticed. This is most probably due to heterogeneities within the sample. For proof-of-principle purposes we consider the average EXAFS profile of the whole ROI.

At this point it is important to retrieve the parameters obtained by an EXAFS profile with this new mode and compare it with that obtained conventionally; by conventionally we mean continuously tuning the energy of incidence with a monochromator until the whole EXAFS spectrum is stored. In that case, the measurement was performed in

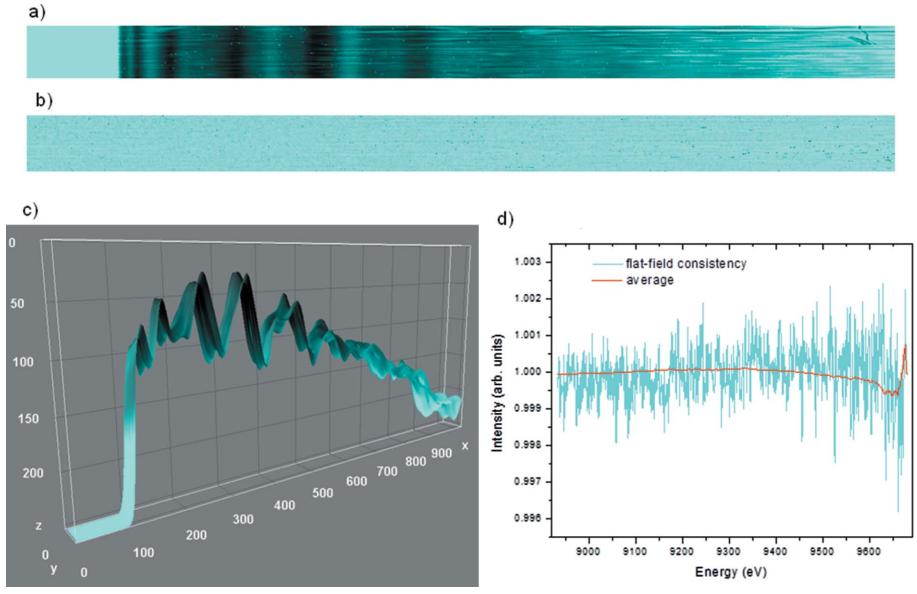

Figure 7
Single-shot EXAFS on a 12.5 µm-thick Cu foil in 6 s. (*a*) Intensity pattern corrected to the flat-field. (*b*) Intensity pattern of the division of two measurements of the flat-field. (*c*) EXAFS profile obtained from the whole illuminated area (1024 × 62 pixels). (*d*) Respective consistency with the average close to unity.

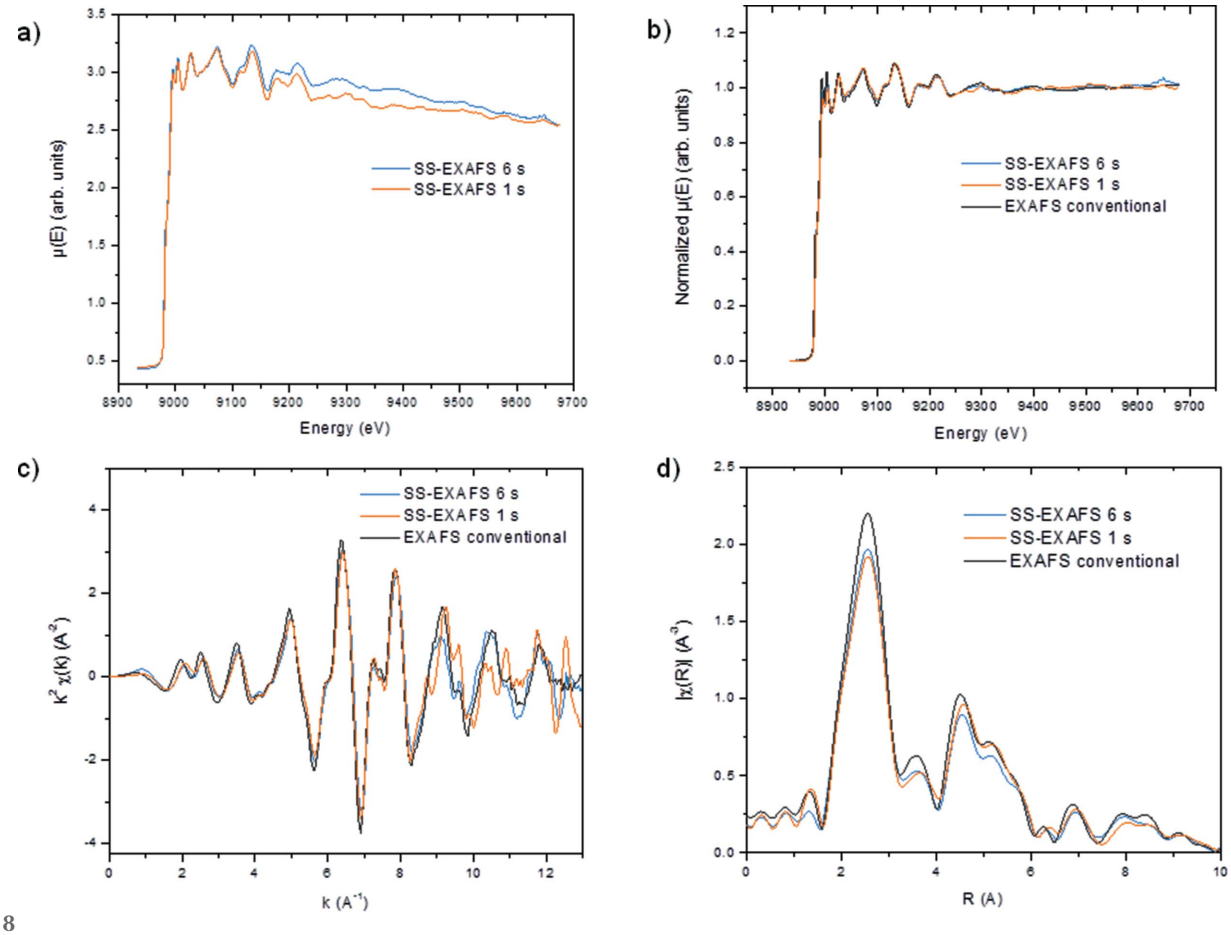

Figure 8
Single-shot EXAFS on a 12.5 µm-thick Cu foil. (*a*) Non-normalized $\mu(E)$ of both 6 s and 1 s acquisition time for the whole EXAFS spectra. (*b*) Normalized $\mu(E)$ of both acquisition times compared with conventionally acquired EXAFS spectrum. (*c*) Wavefunctions and (*d*) respective Fourier-transformed data into *R*.

transmission with two ionization chambers with an acquisition time of 35 min. The 12.5 µm-thick Cu foil was measured for 6 s and 1 s. The average single-shot EXAFS spectra were corrected to flat-field and loaded into *Athena* software (Ravel & Newville, 2005) for the data evaluation. Fig. 8(*a*) shows the untreated and non-normalized EXAFS spectra obtained in 6 s and 1 s. There is practically no change in the signal-to-noise ratio between both spectra. Afterwards a pre-edge and post-edge normalization was applied and the resulting normalized spectra were plotted together with a conventionally measured spectrum of the same foil (Fig. 8*b*). No differences in the absorption features are observed.

Fig. 8(*c*) shows the three spectra plotted in terms of the wavenumber (k), where the amplitude of the absorption features is highlighted. It is visible that the signal-to-noise ratio worsens from about $k = 8$ Å^{-1} for the single-shot EXAFS. Since the absorption features become weaker with increasing k, the sensitivity of the CCD is also lower. However, Fourier-transforming the data using a window just until $k = 8$ Å^{-1} allows quite reliable data to be obtained up to three coordination shells (until approximately 6 Å), when comparing with the conventional-EXAFS spectrum (visible in Fig. 8*d*). However, there is a slight decrease in amplitude (mainly of the first shell at 2.2 Å). This is most probably related to heterogeneities within the sample, since we took the average signal for this purpose.

4. Conclusions and future work

A new and alternative approach to already existent time-resolved XAFS set-ups was presented. For the first time, time- and simultaneous lateral-resolved XAFS measurements were successfully carried out. One of the most important highlights of this set-up is providing a larger area of analysis in one shot (8–10 mm). This allows stratified-like samples to be analyzed, in which differences in the oxidation state or even local coordination environment can be investigated in one shot.

The tests on metal reference foils show that a time resolution of a few seconds with good signal-to-noise ratios is feasible with this set-up given that the sample absorbs strongly enough (edge jump of at least 4).

In the near future, *in situ/operando* investigations on heterogeneous catalysis are planned. Not having to use a micrometer-sized spot is actually an advantage for performing such studies, especially in stratified-like samples.

Taking into account that the photon flux had to be diminished to avoid overload on the pnCCD chip, measurements with a laboratory X-ray tube are feasible. This means that

both time- and spatial-resolved XAFS experiments become possible with laboratory sources, even with low power X-ray sources. Furthermore, low scattering and the 'single-photon-count' mode of the CXC are attractive features for the laboratory.

This manuscript shows the feasibility of this new alternative for single-shot XAFS at the synchrotron. The set-up has been tested by means of metallic reference foils and iron oxide compounds. In the near future the set-up can be tested on an on-going reaction, where parameters like temperature can be adjusted for triggering a mechanism while analyzing *in situ*.

Acknowledgements

The authors wish to thank Anke Kabelitz (BAM) for preparing the Fe_xO_x samples and Monika Klinger (BAM) for the technical drawings of the 'wafer bender'.

References

Bare, S. R., Kelly, S. D., Ravel, B., Greenlay, N., King, L. & Mickelson, G. E. (2010). *Phys. Chem. Chem. Phys.* **12**, 7702–7711.

Bhattacharyya, D., Poswal, A. K., Jha, S. N., Sangeeta & Sabharwal, S. C. (2009). *Nucl. Instrum. Methods Phys. Res. A*, **609**, 286–293.

Bordiga, S., Groppo, E., Agostini, G., van Bokhoven, J. A. & Lamberti, C. (2013). *Chem. Rev.* **113**, 1736–1850.

Bunker, G. (2010). *XAFS – A Practical Guide to X-ray Absorption Fine Structure Spectroscopy*. Cambridge University Press.

D'Acapito, F., Boscherini, F., Marcelli, A. & Mobilio, S. (1992). *Rev. Sci. Instrum.* **63**, 899–901.

Flank, A. M., Fontaine, A., Jucha, A., Lemonnier, M., Raoux, D. & Williams, C. (1983). *Nucl. Instrum. Methods Phys. Res.* **208**, 651–654.

Frahm, R., Stötzel, J. & Lützenkirchen-Hecht, D. (2009). *Workshop on Energy Dispersive X-ray Absorption Spectroscopy Scientific Opportunities and Technical Challenges*, p. 23. ESRF, Grenoble, France.

Gawelda, W. (2006). Thesis, Faculté des Sciences de Base, Lausanne, Switzerland.

Hagelstein, M., Cunis, S., Frahm, R., Niemann, W. & Rabe, P. (1989). *Physica B*, **158**, 324–325.

Kleymenov, E., Sa, J., Abu-Dahrieh, J., Rooney, D., van Bokhoven, J. A., Troussard, E., Szlachetko, J., Safonova, O. V. & Nachtegaal, M. (2012). *Catal. Sci. Technol.* **2**, 373–378.

Koziej, D., Hübner, M., Barsan, N., Weimar, U., Sikora, M. & Grunwaldt, J. D. (2009). *Phys. Chem. Chem. Phys.* **11**, 8620–8625.

Labiche, J. C., Mathon, O., Pascarelli, S., Newton, M. A., Ferre, G. G., Curfs, C., Vaughan, G., Homs, A. & Carreiras, D. F. (2007). *Rev. Sci. Instrum.* **78**, 091301.

Newville, M. (2004). *Fundamentals of XAFS*. University of Chicago, Chicago, IL, USA.

Ordavo, I., Ihle, S., Arkadiev, V., Scharf, O., Soltau, H., Bjeoumikhov, A., Bjeoumikhova, S., Buzanich, G., Gubzhokov, R., Günther, A., Hartmann, R., Holl, P., Kimmel, N., Kühbacher, M., Lang, M., Langhoff, N., Liebel, A., Radtke, M., Reinholz, U., Riesemeier, H., Schaller, G., Schopper, F., Strüder, L., Thamm, C. & Wedell, R. (2011). *Nucl. Instrum. Methods Phys. Res. A*, **654**, 250–257.

Pascarelli, S., Aquilanti, G., Dubrovinsky, L., Guilera, G., Mathon, O., Muñoz, M., Newton, M. A., Pasquale, M. & Trapananti, A. (2006). *Proceedings of the 13th International Conference on X-ray Absorption Fine Structure (XAFS13)*, 9–14 July 2006, Stanford, California, USA.

Pascarelli, S., Neisius, T. & De Panfilis, S. (1999). *J. Synchrotron Rad.* **6**, 1044–1050.

Ravel, B. & Newville, M. (2005). *J. Synchrotron Rad.* **12**, 537–541.

Riesemeier, H., Ecker, K., Görner, W., Müller, B. R., Radtke, M. & Krumrey, M. (2005). *X-ray Spectrom.* **34**, 160–163.

Schäfers, F. (2008). *The BESSY Raytrace Program RAY*, *Springer Series in Modern Optical Sciences: Modern Developments in X-ray and Neutron Optics*, Vol. 137, edited by A. Erko, M. Idir, Th. Krist & A. G. Michette, pp. 9–41. Berlin/Heidelberg: Springer.

Scharf, O., Ihle, S., Ordavo, I., Arkadiev, V., Bjeoumikhov, A., Bjeoumikhova, S., Buzanich, G., Gubzhokov, R., Günther, A., Hartmann, R., Kühbacher, M., Lang, M., Langhoff, N., Liebel, A., Radtke, M., Reinholz, U., Riesemeier, H., Soltau, H., Strüder, L., Thünemann, A. F. & Wedell, R. (2011). *Anal. Chem.* **83**, 2532–2538.

Schneider, C. A., Rasband, W. S. & Eliceiri, K. W. (2012). *Nat. Methods*, **9**, 671–675.

Stötzel, J., Lützenkirchen-Hecht, D. & Frahm, R. (2011). *J. Synchrotron Rad.* **18**, 165–175.

Williams, S. H., Hilger, A., Kardjilov, N., Manke, I., Strobl, M., Douissard, P. A., Martin, T., Riesemeier, H. & Banhart, J. (2012). *J. Instrum.* **7**, P02014.